

RECENT PROGRESS IN GaN-BASED TERAHERTZ SOURCES: A REVIEW

Prof. Dr. **Vadim SIRKELI**

Faculty of Physics and Engineering, Moldova State University

PROGRESE RECENTE ÎN SURSELE TERAHERTZ BAZATE PE GaN

În lucrare sunt prezentate proprietățile fundamentale, mecanismele de creștere a cristalelor și principiile de funcționare a dispozitivelor Terahertz (THz) bazate pe compușii III-N. Este descrisă evoluția și nivelul de dezvoltare a proceselor de obținere a heterojuncțiunilor bazate pe GaN (polar și non-polar) și proprietățile acestora. Autorul analizează în detalii rolul polarizării spontane și piezoelectrice în structurile III-N și impactul lor asupra performanțelor dispozitivelor THz. Sunt trecute în revistă realizările cercetărilor teoretice și experimentale ce țin de QCL, RTD și diode Gunn în baza GaN pentru frecvențe din regiunea THz. După cum se demonstrează, compușii semiconductori pe baza de GaN reprezintă materiale deosebit de prețioase pentru fabricarea surselor THz ce funcționează la temperaturi de până la temperatura camerei, datorită proprietăților sale unice: valoarea mare a lărgimii benzii interzise și a offset-ului benzii de conducție, energia mare a fononilor LO și stabilitatea înaltă la străpungere în câmp electric de intensitate mare. A fost stabilit că sursele THz în bază de GaN acoperă domeniul de frecvențe 5-12 THz, o proprietate foarte importantă pentru imagistica THz și detectarea materialelor explozibile, domenii ce nu pot fi acoperite de dispozitive THz convenționale în bază de GaAs. Reieșind din realizările de ultimă oră privind fabricarea heterostructurilor în bază de GaN (non-polar m-plane) și a dispozitivelor cu densitate joasă de defecte, se conturează o perspectivă clară pentru design-ul și fabricarea surselor THz de putere mare bazate pe GaN (non-polar m-plane) cu posibilitate de funcționare la temperatura camerei.

Cuvinte-cheie: GaN, THz, unde milimetrice, spectroscopie imagistică, caracterizare, laser cuantic în cascadă, rezistență diferențială negativă, diodă tunel cu structură rezonantă, diodă Gunn.

Summary. This paper reviews the crystal growth, basic properties, and principle of operation of III-nitride based terahertz devices. We provide a brief history and current status of crystal growth of polar and non-polar GaN-based heterostructures and its properties. The role of spontaneous and piezoelectric polarization in polar III-nitride structures and its impact on performance of terahertz devices is discussed in detail. In this paper we report on the recent progress of the theoretical and experimental studies of GaN-based THz QCLs, RTDs and Gunn diodes. We show that GaN-based semiconductor compounds are promising materials for fabrication terahertz sources operating up to room temperature due to their unique properties such as large bandgap and conduction band offset (CBO) energy, high LO-phonon energy, and high resistant to the high breakdown electric field. Moreover, it was established that the GaN-based terahertz sources can cover the spectral region of 5-12 THz, which is very important for THz imaging and detection of explosive materials, and which could be not covered by conventional GaAs-based terahertz devices. In terms of the reported significant progress in growth of non-polar m-plane GaN-based heterostructures and devices with low density defects, it is open a wide perspective towards design and fabrication of non-polar m-plane GaN-based high power terahertz sources with capabilities of operation at room temperature.

Keywords: GaN, terahertz, millimeter wave, imaging, spectroscopy, characterization, quantum-cascade lasers, negative differential resistance, resonant tunneling diodes, Gunn diodes.

I. INTRODUCTION

Terahertz (THz) waves refer to the electromagnetic radiation in the frequency range from 0.1 to 10 THz, which corresponds to the wavelengths from 3 mm to 30 μm , respectively [1]. This spectral region, called also as “T-gap”, is important for many practical applications, including THz imaging, chemical and biological sensing, high-speed telecommunication, heterodyne receiver for astronomy, security and other applications [1, 2]. Moreover, THz spectral region covers intermolecular vibrations of biological molecules and low frequency crystalline lattice vibrations of chemical materials, including drugs, explosive and

related compounds (ERCs) such as TNT, RDX, HMX, PETN and other explosive materials [2, 3]. Transmitted and reflectance THz spectra of these materials contain specific THz absorption peaks (finger-prints), which characterize vibration modes of these materials and provide information which could be used for identification of the ERC, and which is not available in the other regions of the electromagnetic spectrum. Leahy-Hoppa et al. [3] are investigated the THz absorption spectra of many explosives and found that the THz absorption peaks (finger-prints) of these explosives are located in the terahertz frequency range of 0.8-6.0 THz. For security applications it is very impor-

Table 1

**THz Absorption Peaks (Finger-prints)
of the explosive materials like RDX, HMX, PETN and TNT [1-3]**

Explosive and related compound	Measured Absorption Peak Position (THz)
RDX	0.82, 1.05, 1.50, 1.96, 2.2, 3.08, 4.3, 5.1, 5.5, 5.95
HMX	1.78, 2.51, 2.82, 3.5, 4.0, 4.8, 5.0, 5.3, 5.5, 5.8, 6.06
PETN	2.0, 2.84, 3.7, 4.3, 4.8, 5.2, 5.5, 5.8
TNT	0.8, 1.1, 1.66, 2.2, 3.69, 4.3, 4.71, 5.52, 6.0

tant to find a reliable, fast, contact-less, and non-destructive method to detect explosive materials such as TNT, RDX, HMX, and PETN. The key THz absorption peaks of these explosives are taken from [1-3] and summarized in table 1.

THz waves have low photon energies (~ 4.1 meV for 1 THz), which is about 1 million times weaker than the energy of X-ray photons, and do neither ignite any explosive materials at typical power levels nor cause any harmful ionization in biological tissues [4]. Thus, THz waves can be considered as a safe method for investigation of biological materials and which can be used in medicine for THz imaging and for other applications.

Despite the great progress in the last few years of design, fabrication and demonstration THz devices based on GaAs/AlGaAs materials, there are some limits of bandgap engineering due to the relatively low (0.72 eV for GaAs/AlAs) conduction band offset (CBO). To overcome the issue of the CBO limits new material systems such as InAs/AlSb, InGaAs/GaAs, ZnO/ZnMgO, ZnSe/ZnMgSe, InGaN/GaN, GaN/AlN and GaN/AlGaN are considered as promising for room-temperature THz sources. Among these materials, the III-nitride compounds are most attractive due to their larger CBO (1.57 eV for GaN/AlN [5,6]) that is crucial for the fabrication of THz QCL lasers with enhanced performance and higher operating temperature. Below we review basic properties, crystal structure and growth of III-nitride materials as well as the recent progress and current status of GaN-based terahertz sources, including the quantum cascade lasers (QCLs), quantum resonant-tunneling diodes (RTDs), and Gunn diodes.

II. GROWTH, CRYSTAL STRUCTURE AND BASIC PROPERTIES OF III-NITRIDES

III-Nitride materials, which include binary compounds InN, GaN, AlN and their alloys, have been investigated last several decades and are among the most important semiconductor materials for photonics, optoelectronics, high-power and high-frequency electronics. These materials have a direct bandgap

and their bandgap energy covers broad spectral range from the near infrared to deep ultraviolet: $E_g = 0.7$ eV for InN, $E_g = 3.4$ eV for GaN, and $E_g = 6.2$ eV for AlN [7]. III-nitride materials can be doped n- and p-types using Si(Ge) or Mg impurities [6], respectively, and can be also grown heteroepitaxially on different foreign substrates, including sapphire, SiC and Si. Contrary to other III-V compounds like InP and GaAs, which have the zinc blende structure, III-nitride binary semiconductors have the wurtzite structure as shown in figure 1 [8].

Wurtzite crystal structure consists of two hexagonal close packed lattices, displaced towards the direction perpendicular to the hexagonal base (c-direction) by $\pm 3c/8$, where c is the lattice parameter [8]. Also, the III-nitrides can be crystallized in the rock-salt [9] and meta-stable zinc blende crystal structures [10]. The wurtzite crystal structures lack of inversion symmetry along the c-direction, which is referred to as a crystallographic polarity. In GaN the c-direction is the polar direction. GaN films can be grown along c-direction in two different polarities: “Ga-polar” ([0001] direction) and “N-polar” ([000 $\bar{1}$] direction), as shown in figure 1. The polarity is the bulk property of GaN, which results in different chemical and physical properties.

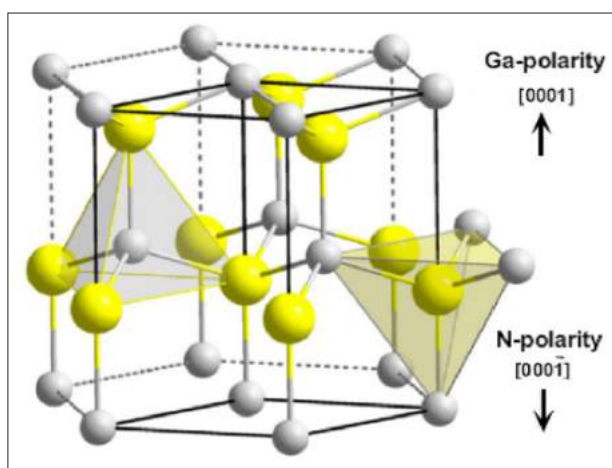


Figure 1. GaN wurtzite crystal structure. Large yellow balls are nitrogen atoms and small grey balls are Ga atoms. Reprinted from Ref. [8].

For the first time GaN was synthesized by Juza and Hahn in 1938 [11]. In 1969 Marushka and Tietjen [12] grown large area thin film GaN on sapphire substrates using the hydride vapor phase epitaxy (HVPE). One of major issues of III-nitride semiconductor materials is the lack of the substrates for homoepitaxial growth of thin films. The most GaN-based devices are grown heteroepitaxially on different foreign substrates including sapphire, silicon carbide and silicon. Due to the lattice mismatch between foreign substrates and III-nitrides a nucleation buffer layer is needed. To overcome this issue and reduce the dislocations density in the grown films several research groups suggested to use the nitridation of the sapphire, or to use the AlN and GaN low temperature buffer layers [13] grown by the molecular beam epitaxy (MBE) or the metal organic chemical vapor deposition (MOCVD) methods.

The all III-nitride materials exhibit spontaneous and piezoelectric polarizations [14], which create internal electric fields and have significant impact on the optical, electronic and transport properties of GaN-based heterostructures and devices. When the III-nitride heterostructures grow along the c -direction and have N-face polarity, the spontaneous polarization field along the c -direction is positive $P_{sp} > 0$. In the opposite case, the spontaneous polarization field is negative $P_{sp} < 0$ when heterostructures have Ga-face polarity. The magnitude of the spontaneous polarization field P_{sp} increases with increasing deviation of the unstrained crystal structure from the ideal closed-packed arrangement (P_{sp} increases in going from GaN to InN to AlN). The piezoelectric polarization field P_{pe} in III-nitride heterostructures grown along c -direction (z -axis) depend on the non-zero elements of the tensor describing the strain state of the crystal [15]:

$$\varepsilon_{xx} = \varepsilon_{yy} = \frac{a - a_0}{a_0}, \quad \varepsilon_{zz} = -2 \frac{C_{13}}{C_{33}} \varepsilon_{xx} \quad (1)$$

where a_0 and a are the equilibrium and strained values of the in-plane lattice constants, respectively, and C_{13} and C_{33} are elastic constants. Piezoelectric polarization field P_{pe} is defined as [15]:

$$P_{pe} = \pm 2 \varepsilon_{xx} \left(\varepsilon_{31} - \varepsilon_{33} \frac{C_{13}}{C_{33}} \right), \quad (2)$$

where ε_j are the piezoelectric coefficients, the plus and minus signs refer to N-face and Ga-face polarities, respectively. For GaN heterostructures with Ga-

face polarity P_{pe} is negative for tensile and positive for the compressive strain. The net polarization density could be defined as the sum of spontaneous and piezoelectric polarizations, i.e. $P = P_{sp} + P_{pe}$. When net polarization density is non-zero in III-nitride-based heterostructures, it creates polarization induced built-in electric field, which tilts the band edges in the multi-quantum well structures. This results in the decreased mutual overlap between electron and hole wave functions in quantum wells and hence reduced spontaneous emission and absorption coefficients. To reduce the built-in electric field caused by spontaneous and piezoelectric polarizations the III-nitride heterostructures could be grown on non-polar or semi-polar foreign substrates.

III. GaN-BASED THz QCLs

Among different types of terahertz sources, the quantum cascade lasers (QCLs) at THz frequencies offer technology platform for the high power generation of THz radiation at room temperature. The QCL was originally proposed by Kazarinov and Sirius in 1971 [16] and was first demonstrated by Faist et al. [17] in the mid-infrared region (70 THz) in 1994 and Köhler et al. [18] in the terahertz region (4.4 THz) in 2002. In general, QCL makes use of electron transitions between subbands formed by multiple strongly coupled quantum wells. By adjusting the widths of the quantum wells/barriers, the emission frequency and performance of the laser can be tailored, adding addi-

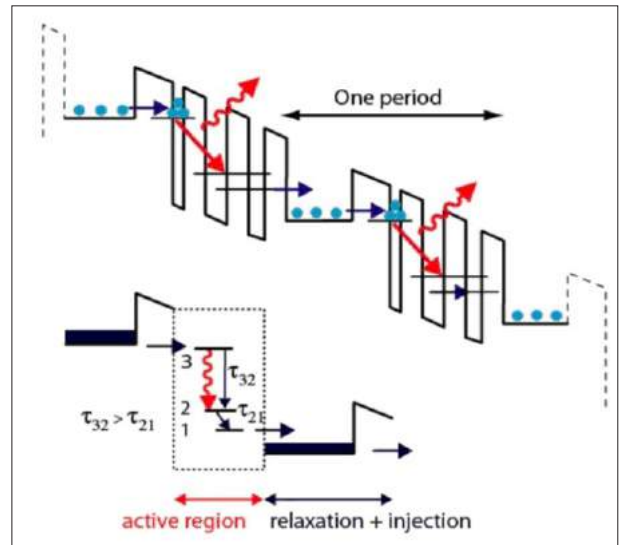


Figure 2. Schematic structure and principle of operation of a quantum cascade laser. The diagram shows the electron energy versus position in the structure, which contains three quantum wells. The overall downward trend of energy towards the right-hand side is caused by an applied electric field.

tional flexibility in the laser design. The QCL operates on optical transitions not between different electronic bands but on intersubband (ISB) transitions of a semiconductor structure, as shown in figure 2.

For practical applications of any lasers, one of the key desired characteristics is room-temperature operation. Mid-IR QCLs with CW room-temperature operations have been demonstrated in spectral coverage from 4.5 to 10 μm [19]. However, THz QCLs have not yet satisfied this requirement. The cryogenic cooling is required, which is the main obstacle towards making THz QCL a compact radiation source. The most successful material system for THz QCL is GaAs/AlGaAs heterostructure grown on GaAs substrate. The present THz QCLs have covered the spectral range 1–5 THz, and maximum operating temperature is about 200 K at a radiation frequency of 3.2 THz [20]. For lower radiation frequency, the best working temperature is about 163 K at 1.8 THz [21] and 69 K at 1.2 THz [22]. With regard to output power, a single state-of-art THz QCL could provide 1 W peak power in pulsed mode [23] and over 130 mW in continuous wave (CW) [24] at 10 K heat-sink temperature. Therefore, the main challenge in this field is to achieve room-temperature THz QCLs which can enable practical applications of THz technology.

Thus, the relatively small LO-phonon energy is an obvious obstacle for further temperature improvement. Among II-VI and III-V semiconductor compounds, GaN/AlGaN seems to be a promising candidate for room temperature (even higher temperature) THz QCL thanks to its much larger LO-phonon energy (92 meV) [5]. Among wide bandgap semiconductors, there is one first major advantage to develop THz quantum cascade devices using the GaN/AlGaN material system in terms of the exceptionally broad spectral range, which can be covered using this material system. Indeed, standard III-V semiconductors like GaAs cannot be operated in the 5-12 THz frequency range because of their Reststrahlen band, i.e. the spectral region where the material is completely opaque due to the absorption by optical phonons. This is not the case for GaN because of the three-fold larger energy of the optical phonons. Thus, GaN offers prospects for THz quantum cascade devices, which can operate in a much broader spectral range from 1 to 15 THz and in particular in the 5-12 THz, which cannot be covered by other III-V semiconductors.

Bellotti et al. [5] theoretically established that the GaN/AlGaN-based THz QCLs could operate up to room temperature. The design of nitride-based THz QCL devices operating at room temperature is more complex than conventional GaAs/AlGaAs devices due

to the spontaneous and piezoelectric polarizations in III-Nitride materials and the lattice mismatch. To overcome this issue, Sara et al. [25] suggested to use of III-Nitride lattice-matched structures for THz QCLs. They reported on numerical simulation study of the carrier interactions and population inversion characteristics of lattice-matched GaN/InAlGaN-based THz QCLs using an ensemble Monte Carlo method. The THz QCL structure consists of GaN quantum well and $\text{Al}_{0.318}\text{In}_{0.0707}\text{Ga}_{0.6113}\text{N}$ barriers. This $\text{GaN}/\text{Al}_{0.318}\text{In}_{0.0707}\text{Ga}_{0.6113}\text{N}$ structure is lattice matched compared to the $\text{GaN}/\text{Al}_{0.15}\text{Ga}_{0.85}\text{N}$ structures from Ref. [5] that is not lattice matched. The bandgap energy of the lattice matched $\text{Al}_{0.318}\text{In}_{0.0707}\text{Ga}_{0.6113}\text{N}$ were interpolated to value of 3.736 eV using the following expression [26]:

$$E_{\text{AlInGaN}}(x, y) = (1 - x - y) \times E_{\text{GaN}} + x \times E_{\text{AlN}} + y \times E_{\text{InN}}, \quad (3)$$

where E_{InN} , E_{GaN} and E_{AlN} correspond to InN, GaN, and AlN band gap energy. The desired x and y values were selected to satisfy the lattice match condition and the conduction band offset is of approximately 200 meV [25]. Conduction band profiles of both $\text{GaN}/\text{Al}_{0.318}\text{In}_{0.0707}\text{Ga}_{0.6113}\text{N}$ and $\text{GaN}/\text{Al}_{0.15}\text{Ga}_{0.85}\text{N}$ THz QCL devices are presented in figures 3(a)-1(b), respectively. The lattice-matched $\text{GaN}/\text{Al}_{0.318}\text{In}_{0.0707}\text{Ga}_{0.6113}\text{N}$ structure contains five energy states (figure 3 (a)) and the layer thicknesses of one cascade of this structure starting from the injector barrier in \AA are: **25/39/19/30/22/53/18/29**. The non-lattice-matched $\text{GaN}/\text{Al}_{0.15}\text{Ga}_{0.85}\text{N}$ structure contains four energy states (figure 3(b)) and the layer thicknesses of one cascade of this structure starting from the injector barrier in \AA are: **26/37/22/31/26/59** starting from the leftmost barrier downstream to the rightmost well.

The authors [25] calculated the fractional population inversion versus temperature for four different QCL structures GaN/AlGaN, $\text{GaN}/\text{Al}_{0.318}\text{In}_{0.0707}\text{Ga}_{0.6113}$, GaAs/AlGaAs and ZnO/MgZnO, which is shown in figure 4. As could be seen from figure 4 the lattice-matched GaN/InAlGaN THz QCL structure has the highest population inversion. It was established that the degradation of population inversion versus temperature in the III-nitride THz QCLs is much less compared to the GaAs/AlGaAs and ZnO/MgZnO QCL structures. Therefore, the III-nitride QCL structures could be appropriate for THz lasing especially if high quality lattice matched structures can be grown.

Terashima et al. [27] reported on successful fabrication of GaN-based THz QCLs employing two-well design scheme with a pure 3-level laser system. They used a radio-frequency molecular beam epitaxy (RF-MBE) technique to grow GaN/AlGaN THz QCL devices. The contact layers were grown on a high-qual-

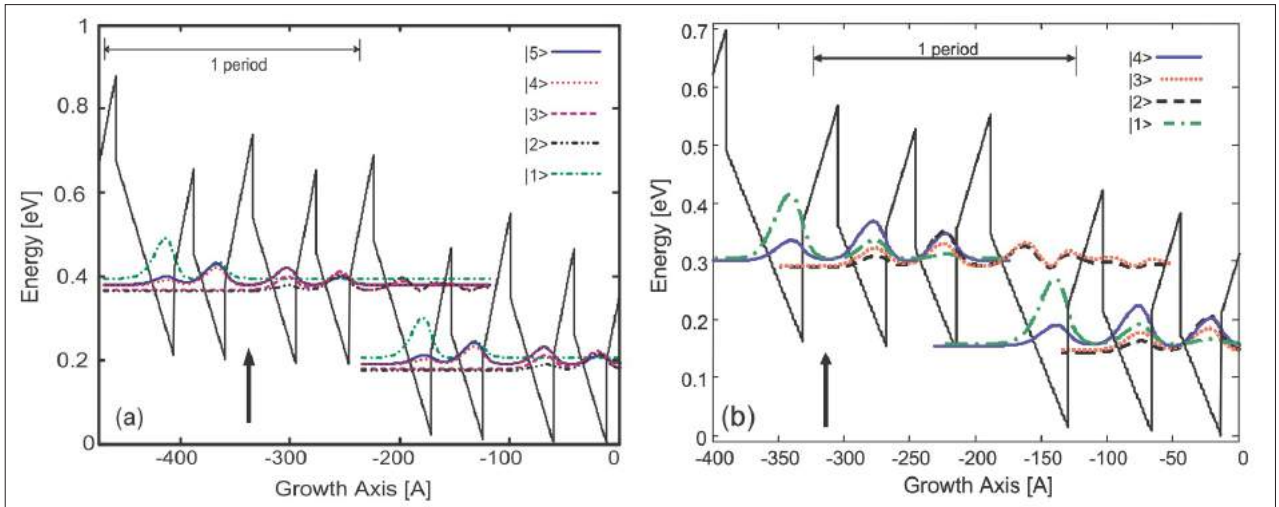


Figure 3. Conduction band profile and squared envelope functions of (a) GaN/Al_{0.318}In_{0.0707}Ga_{0.6113}N THz QCLs simulated in Ref. [25] and (b) GaN/Al_{0.15}Ga_{0.85}N THz QCL obtained from Ref [5]. Reprinted from Ref. [25].

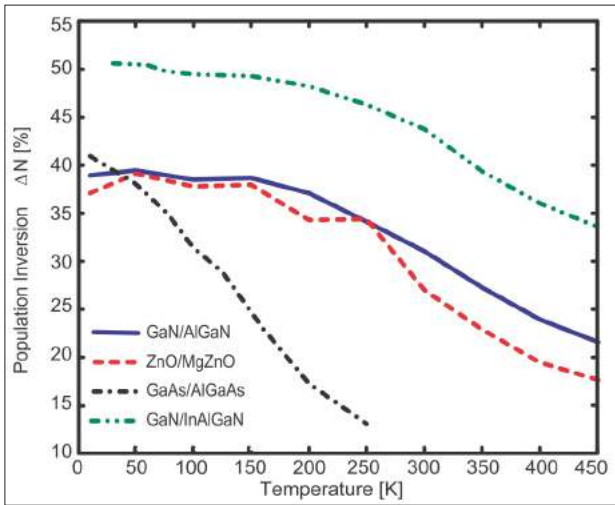


Figure 4. Population inversion for 4 different QCL structures versus temperature. Reprinted from Ref. [25].

ity c-plane AlGaN/AlN templates, which itself was grown on c-plane sapphire substrate by metallo-organic chemical vapor deposition (MOCVD) technique. To achieve the population inversion condition, the 6 nm thick GaN wells were doped by Si with concentration of $5 \times 10^{17} \text{ cm}^{-3}$. The QCL has a ridge structure with a resonant length of 1.14 mm and a width of 120 μm . The authors used a single metal waveguide structure, which was mounted on a gold-nickel heat sink, as shown in figure 5.

The frequency spectrum of this GaN-based QCL in pulse mode (with 200 ns pulse width), recorded at 5.6 K, is shown in figure 3. As can be seen in Figure 6, the peak frequency of 5.47 THz was observed in the laser spectrum of this GaN-based QCL device with threshold current, threshold current density, and the threshold voltage of 3.5A, 2.75kA/cm², and 16.5V, respectively.

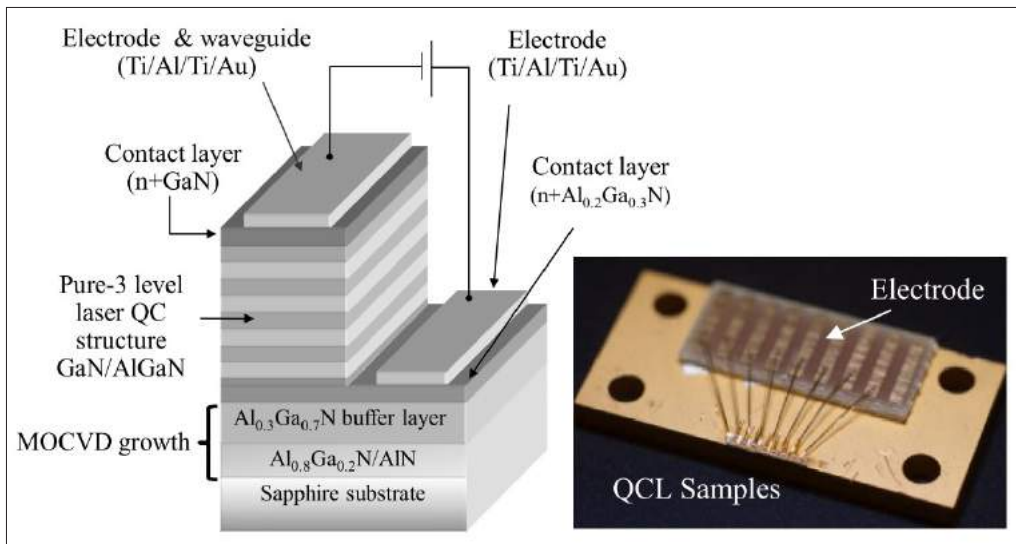


Figure 5. Schematic diagram for the overall structure of a GaN-based THz QCL and a photograph of the THz QCL samples mounted on a gold-nickel heat sink. Reprinted from Ref. [27].

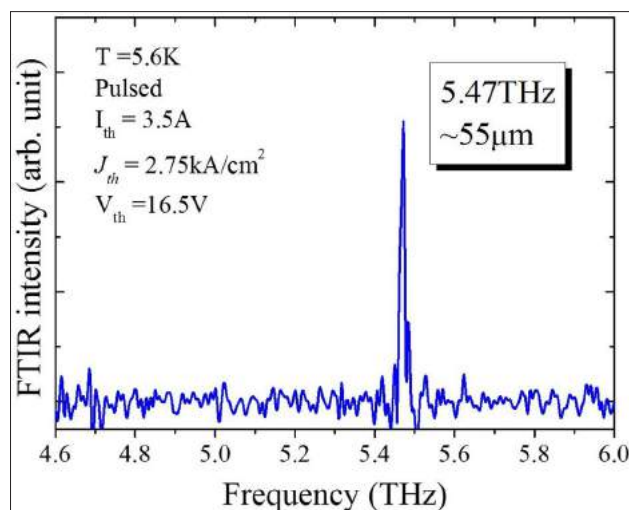


Figure 6. Fourier transform IR frequency spectrum obtained from a GaN-based THz QCL with a pure three-level design. The lasing spectrum has a peak frequency of 5.47 THz and wavelength of 55 μm . Reprinted from Ref. [27].

IV. GaN-BASED THz RESONANT TUNNELING DIODES

Among different types of electronic devices, the resonant tunneling diodes (RTDs) are promising candidate for terahertz wave generation and amplification, for signal detection and frequency mixing, all at room temperature. The RTD is a quantum-effect semiconductor device using quantum mechanical tunneling. Its operating principle is based on the resonant tunneling effect proposed by Tsu and Esaki in 1973 [28]. The conduction-band profiles of a conventional RTD and their relation to current-voltage characteristics are schematically shown in figure 7 [29]. The case under zero bias is shown in figure 7(a). The RTD's active layers consist of a double barrier (DB) structure where an undoped quantum well layer is sandwiched between two undoped barrier layers with on the order of 1 nm thick. The DB layers are connected with heavily doped emitter and collector contact regions filled with electrons. Discrete quasi-bound or resonant levels are formed in the well layer. In figure 7(a), the lowest resonant level is indicated. As the bias voltage increases, electrons flow from the emitter to the collector through the resonant level. The current increases almost linearly until the emitter's conduction band edge exceeds the resonant level, as shown in figure 4(b). A further increase in the bias voltage causes a sharp drop in the current because the resonant level falls below the emitter's conduction band edge, as shown in figure 7(c). The current-voltage characteristics in figure 7(d) exhibit negative differential conductance (NDC), which is one of the most important features

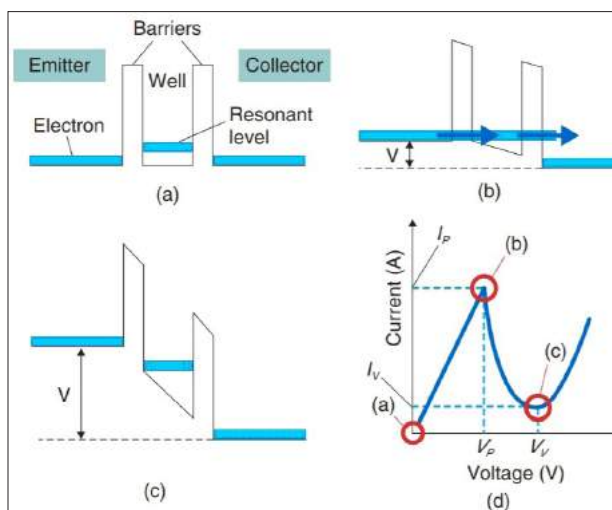


Figure 7. Conduction band profiles of a RTD at three different bias voltages (V): (a) zero bias ($V=0$), (b) resonance ($V=V_p$), and (c) off-resonance ($V=V_v$). (d) Schematic current-voltage characteristics of a DB RTD.

Reprinted from Ref. [29]

of RTDs. The ratio of peak current to valley current (I_p/I_v) in figure 7(d) is called the peak-to-valley ratio (PVR) and is one of the figures of merit of RTDs.

In the last decade, significant progress has been made in the design and fabrication of THz RTDs based on AlGaAs/GaAs, InGaAs/AlAs, InGaAs/InAs and AlGaN/GaN material systems. In 2012 Feiginov *et al.* [30] reported on experimental fabrication of RTDs based on InGaAs/InAs/ InGaAs with heavily doped collectors where they achieved a maximum operating frequency of 1.1 THz. In 2016 Maekawa *et al.* [31] reported on the achievement of a large increase in oscillation frequency up to 1.92 THz in InGaAs-based RTDs by reducing the conduction loss. A maximum output power of 0.61 mW at 620 GHz, 20-30 μW at 1 THz, and 0.4 μW at 1.92 THz were obtained for InGaAs-based RTD structures with slot antenna and two-array configuration and reported in Refs. [31]. To enhance frequency performance of THz RTDs several approaches have been suggested, including the design schemes with step-graded emitter (figure 8) [29, 31], with variable barrier heights and RTDs with double-well triple barriers [32].

Thus, increasing the output power of RTD devices at THz frequencies and increasing the operation frequency are crucial tasks. To solve these, GaN-based compounds are explored as materials for high-power terahertz emitter devices due to the higher CBO (1.57 eV for GaN/AlN vs. 0.72 for GaAs/AlAs) [5].

In the last two decades resonant tunneling transport has been extensively studied in the GaN/AlGaN double-barrier structures [33, 34]. In the first reports [33] it was found that the current-voltage characteris-

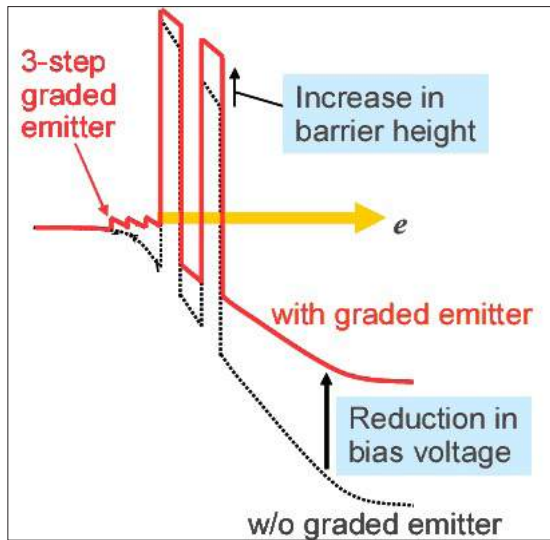


Figure 8. Conduction band profiles of RTDs with 3-step graded emitter and without graded emitter. Reprinted from Ref. [29].

tics of GaN-based RTD structures have a strong hysteresis and it rapidly degrades upon repeated voltage scans. This behavior of current-voltage dependences of the GaN-based RTDs is generally attributed to filling of traps related to threading dislocations. In later papers [34] it was reported on stable and repeatable NDR feature in the current-voltage dependence of GaN-based RTD, which was grown under conditions minimizing the formation of strain-induced defects. Also, the sequential tunneling transport in a simple GaN/AlGaIn quantum cascade structures has been investigated, and it was found that current-voltage characteristics of such structures have a highly non-linear behavior [35]. Moreover, also in paper [36] it was found that experimental turn-on voltages are well reproduced by simulation results. Also authors [36] reported on the observation of electroluminescence peak at near 10 THz, which is related to the photon-assisted tunneling process in the active QWs. Terashima et al. [35] reported on more significantly stronger emission at 1.4 THz, which was observed in the GaN-based quantum cascade structures and attributed to the intersubband (ISB) transitions in QCL structures. In recent paper Encomendero et al. [37] reported on the room-temperature generation of microwave oscillations from GaN/AlN RTDs, which exhibit record-high current densities up to 220 kA/cm² with an output power of 3 μW. The RTD devices were grown by molecular beam epitaxy (MBE) method on freestanding GaN substrates with nominal dislocation densities <math> < 5 \times 10^4 \text{ cm}^{-2}</math>. The active of the RTDs consists of two 2 nm-thick AlN barriers and a 1.75 nm-wide GaN quantum well, which confines the res-

onant states. The authors found that the fundamental oscillation frequency of such RTDs is ~0.94 GHz with output power of 3 μW, which is limited by the RC of the external biasing circuit. Using the small-signal equivalent circuit model of RTD devices [32], the authors estimated a maximum oscillation frequency $f_{\text{max}} \sim 0.2$ THz. This value of the maximum oscillation frequency is within the same order of magnitude as the values of f_{max} obtained from GaAs/AlAs and InGaAs/AlAs RTD devices [30, 31]. Moreover, reducing the series resistance with improved ohmic contacts and by further optimization of the doping level and collector space width, the capacitance of the GaN-based RTD devices could be significantly reduced [38], and thus achieving the oscillation frequency with $f_{\text{max}} \sim 1$ THz.

V. GaN-BASED THz GUNN DIODES

Gunn diodes represent another type of semiconductor structures, which are conventionally used for generation of high-frequency microwave signals due to the presence of negative differential resistance (NDR) feature in current-voltage characteristics of such devices. GaAs and InP are conventional semiconductor materials used for fabrication of Gunn diodes. GaAs has an energy-relaxation time of 10 ps and exhibits sharp suppression in output power of microwave emission with frequencies higher than 100 GHz. In contrast to GaAs, GaN has a shorter energy relaxation time among III-V semiconductors and exhibits the NDR effect in the threshold fields above 80 kV/cm [39]. GaN-based Gunn diodes have a higher electron velocity and reduced time constants compared to conventional GaAs-based Gunn diodes. Therefore, GaN-based Gunn diodes can generate microwaves with THz frequencies.

The first GaN-based Gunn diodes were fabricated by researchers from the University of Michigan in 2000 [40]. They used a 3 μm thick GaN active layer with an electron concentration of $1 \times 10^{17} \text{ cm}^{-3}$ sandwiched between anode and cathode, which have been made of 0.1 μm thick GaN layer n-type doped with concentration of $1 \times 10^{19} \text{ cm}^{-3}$, as shown in figure 9(a). The diameter of fabricated Gunn diode was 50 μm and the output power of GaN-based Gunn diodes was up to four times higher than that of GaAs-based devices. The NDR relaxation frequency was estimated to be ~1 THz for GaN-based devices for inter-valley transfer-based NDR, and ~4 THz for the inflection-based NDR devices (figure 9(b)) [40]. These values of microwaves frequencies are about one order of magnitude higher than that for GaAs-based NDR devices ($f_{\text{NDR}} \sim 100$ GHz for GaAs-based NDR devices) [40].

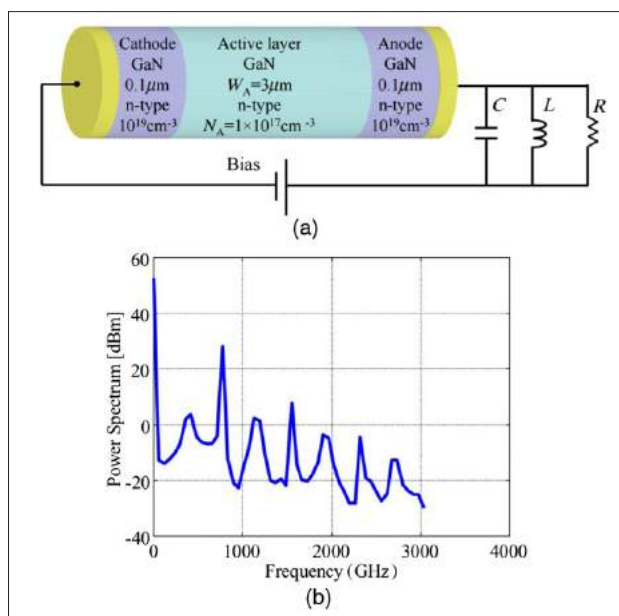


Figure 9 (a). Schematic of GaN NDR diode oscillator. (b) Simulated output power spectrum of THz GaN-based NDR oscillator [40]. Reprinted from Ref. [40].

In 2016 Wang et al. [41] proposed a GaN-based planar Gunn diode. On the interface of GaN/AlGaN heterostructures a two-dimensional degenerated (2DEG) electron gas is formed with high electron concentration, which is beneficial for the fast formation of the dipole domain layer. This results in enhancing the microwave-frequency output power. The electron concentration in this region is higher than that in other regions, and also it acts as a n+-doped layer of GaN-based Gunn diode. The structure of this GaN-based planar Gunn diode is similar to the structure of GaN-based high electron mobility transistor (HEMT), which is shown in figure 10 [41].

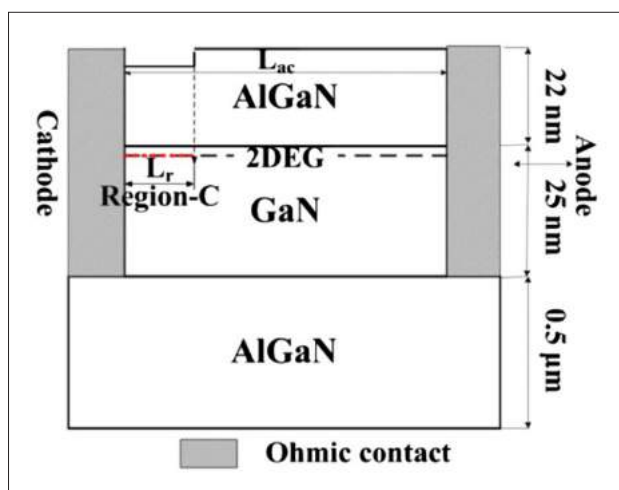


Figure 10. The schematic structure of GaN-HEMT like planar Gunn diode. Reprinted from Ref. [41].

VI. CONCLUSION

In this paper, we have provided a comprehensive review of the recent progress and current status of terahertz sources based on III-nitride semiconductor compounds. It was established that GaN-based semiconductor compounds are promising materials for the fabrication of terahertz sources operating up to room temperature due to their unique properties such as large bandgap and CBO energies, high LO-phonon energy, and high breakdown electric field. Moreover, the GaN-based terahertz sources can cover the spectral region of 5-12 THz, which is very important for THz imaging and detection of explosive materials, and which could be not covered by conventional GaAs-based terahertz devices. This paper includes a review of theoretical and experimental study of GaN-based THz QCLs, RTDs and Gunn diodes. Recent papers report on significant progress in growth of non-polar m-plane GaN-based heterostructures and devices with low density of defects and solving one of the main issues of polar c-plane grown nitride materials - the presence of spontaneous and piezoelectric polarizations in such structures. Thus, a wide perspective is open to design and fabricate non-polar m-plane GaN-based high power terahertz sources, and to achieve room temperature operation.

ACKNOWLEDGEMENTS

V.P.S. gratefully acknowledges financial support from the Alexander von Humboldt Foundation. This work was also partly supported under Institutional Project 15.817.02.34A. The author would like to thank Acad. Prof. Dr. Ion Tiginyanu and Prof. Dr. Hans Hartnagel for their helpful advice, discussion of the manuscript and comments. The author, however, bears full responsibility for this review paper.

REFERENCES

1. Williams B. S. In: Nature Photonics 1, 517-525 (2007).
2. Sirkeli V. P. et al. In: Sensor Letters 16, 1-7 (2018).
3. Leahy-Hoppa M. R. et al. In: Chemical Physics Letters 434, 227-230 (2007).
4. Scarfi M. R. et al. In: J. Biol. Phys. 29, 171-177 (2003).
5. Bellotti E. et al. In: J. Appl. Phys. 105, 113103 (2009).
6. Sirkeli V. P. et. al. In: Journal of Physics D: Applied Physics 50, 035108 (2017).
7. Morkoc H., Gallium Nitride (GaN) I. In: Semiconductors and Semimetals. vol. 50, ed. J. I. Pankove and T. D. Moustakas (San Diego: Academic) ch. 8 (1998).
8. File: https://commons.wikimedia.org/wiki/file:Wurtzite_polyhedra.png - Wikipedia, the free encyclopedia.
9. Xia Q. et al. In: J. Appl. Phys. 73, 8198 (1993).

10. Lei T. et. al. In: J. Appl. Phys. 71, 4933 (1992).
11. Juza R. et al. In: Anorg. Allgem. Chem. 234, 282 (1938).
12. Maruska H. P., Tietjen, J. J. In: Appl. Phys. Lett. 15, 367 (1969).
13. Mikroulis S. et al. In: Appl. Phys. Lett. 80, 2886 (2002).
14. Bernardini F. et. al. In: Phys. Rev. B 56, R10024 (1997).
15. Chuang S. L. In: Physics of Photonic Devices (Hoboken: Wiley) (2009).
16. Kazarinov R. F., Suris, R. A. In: Fiz. Tekh. Populovod. 5, 797-800 (1971).
17. Faist J. et al. In: Science 264, 553-556 (1984).
18. Köhler R. et al. In: Nature 417, 156-159 (2002).
19. Yao Y. et. al., Mid-infrared quantum cascade lasers. In: Nature Photon. 6, 432-439 (2012).
20. Fathololoumi S. et. al. In: Opt. Express 20, 3331-3339 (2012).
21. Kumar S. et. al. In: Nature Phys. 7, 166-171 (2010).
22. Walther C. et. al. In: Appl. Phys. Lett. 91, 131122 (2007).
23. Li L. et. al. In: Electron. Lett. 50, 309-311 (2014).
24. Williams B. S. In: Electron. Lett. 42, 89-91 (2006).
25. Shishehchi S. et al. In: Proc. of SPIE 8980, 89800T (2014).
26. E. Sakalauskas E. et al. In: J. Appl. Phys. 110, 01302 (2011).
27. Terashima W. et al. In: Proc. of SPIE 9483, 948304 (2015).
28. Tsu R., Esaki L. In: Appl. Phys. Lett. 22, 562-564 (1973).
29. Sugiyama H. et al. In: NTT Technical Review 9, 1-7 (2011).
30. Feiginov M. et al. Proc. of SPIE 8496, 84960A (2012).
31. Maekawa T. et al. In: Appl. Phys. Express 9, 024101 (2016).
32. Sirkeli V. P. et al. In: IEEE Transactions on Electron Devices 64, 3482-3488 (2017).
33. Kikuchi A. et. al. In: Appl. Phys. Lett. 81, 1729-1731 (2002).
34. Li D. et. al. In: Appl. Phys. Lett. 100, 252105 (2012).
35. Sudradjat F. et. al. In: J. Appl. Phys. 108, 103704 (2010).
36. Terashima W., Hirayama, H. In: Phys. Status Solidi C 8, 2302 (2011).
37. Encomendero J. et al. In: Appl. Phys. Lett. 112, 103101 (2018).
38. H. Kanaya H. et al. In: J. Infrared, Millimeter, Terahertz Waves 35, 425 (2014).
39. Krishnamurthy S. et al., In: Appl. Phys. Lett. 71, 1999-2001 (1997).
40. Alekseev E. et al. In: Proc. of the 11th Int. Symp. on Space Terahertz Technology, p. 162 (2000).
41. Wang Y. et al. In: Phys. Status Solidi C 13, 382-385 (2016).



Ada Zevin. *Flori de toamnă*, 1993, u/p, 65 × 60 cm